Structural and Thermodynamic Characterization of Polyphenylbenzenes

ARTICLE *in* THE JOURNAL OF PHYSICAL CHEMISTRY A · SEPTEMBER 2011

Impact Factor: 2.69

6 AUTHORS, INCLUDING:

Carlos F R A C Lima
University of Porto
38 PUBLICATIONS **262** CITATIONS
SEE PROFILE

André Melo
University of Porto
55 PUBLICATIONS **385** CITATIONS
SEE PROFILE

Ligia R. Gomes
University of Porto
103 PUBLICATIONS **843** CITATIONS
SEE PROFILE

Luís M N B F Santos
University of Porto
237 PUBLICATIONS **3,681** CITATIONS
SEE PROFILE

THE JOURNAL OF PHYSICAL CHEMISTRY A

ARTICLE

pubs.acs.org/JPCA

Structural and Thermodynamic Characterization of Polyphenylbenzenes

Carlos F. R. A. C. Lima,[†] Marisa A. A. Rocha,[†] André Melo,[‡] Lígia R. Gomes,[‡,§] John N. Low,[∥] and Luís M. N. B. F. Santos*[,†]

[†]Centro de Investigação em Química, Departamento de Química e Bioquímica, Faculdade de Ciências da Universidade do Porto, P-4169-007 Porto, Portugal

[‡]REQUIMTE - Departamento de Química e Bioquímica, Faculdade de Ciências, Universidade do Porto, Rua do Campo Alegre, P-4169-007, Porto, Portugal

[§]CIAGEB - Faculdade de Ciências da Saúde, Escola Superior de Saúde da UFP, Universidade Fernando Pessoa, P-4200-150 Porto, Portugal

[∥]Department of Chemistry, University of Aberdeen, Meston Walk, Old Aberdeen, AB24 3UE, Scotland

Supporting Information

ABSTRACT: The thermodynamic and structural study of a series of polyphenylbenzenes, from benzene, n(Ph) = 0, to hexaphenylbenzene, n(Ph) = 6, is presented. The available literature data for this group of compounds was extended by the determination of the relevant thermodynamic properties for 1,2,4-triphenylbenzene, 1,2,4,5-tetraphenylbenzene, and hexaphenylbenzene, as well as structural determination by X-ray crystallography for some of the studied compounds. Gas phase energetics in this class of compounds was analyzed from the derived standard molar enthalpies of formation in the gaseous phase. The torsional profiles relative to the phenyl−phenyl hindered rotations in some selected polyphenylbenzenes, as well as the gas phase structures and energetics, were derived from quantum chemical calculations. In the ideal gas phase, a significant enthalpic destabilization was observed in hexaphenylbenzene relative to the other polyphenylbenzenes, due to steric crowding between the six phenyl substituents. A relatively low enthalpy of sublimation was observed for hexaphenylbenzene, in agreement with the decreased surface area able to establish intermolecular interactions. The apparently anomalous low entropy of sublimation observed for hexaphenylbenzene is explained by its high molecular symmetry and the six highly hindered phenyl internal rotations. For the series of polyphenylbenzenes considered, it was shown that the differentiation in the entropy of sublimation can be chiefly ascribed to the torsional freedom of the phenyl substituents in the gas phase and the entropy terms related with molecular symmetry.

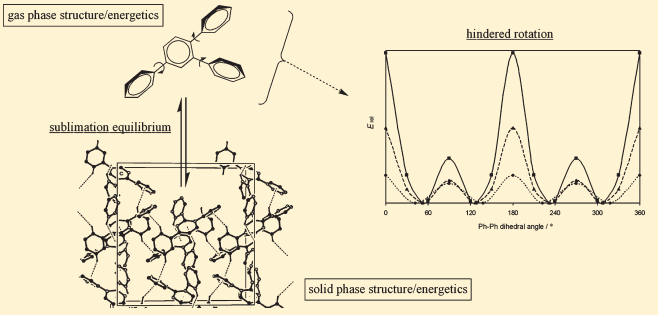

1. INTRODUCTION

Polyphenylbenzenes are benzene derivatives with the general formula presented in Figure 1. The phenyl substituents may have other groups attached to them and are distributed around a central benzene ring. In this work, polyphenylbenzenes bearing simple phenyl substituents, from benzene, n(Ph) = 0, to hexaphenylbenzene, n(Ph) = 6, are considered.

Polyphenylbenzenes possess the ability to form conducting polymers[1,2] and have some applications in the fields of organic light emitting diodes (OLEDs) and nonlinear optical devices,[3,4] field-effect transistors, ultraviolet organic lasers,[5] catalysis,[6,7] and enzyme simulation[8] among others. Some polyphenylbenzene derivatives have biological activities, behaving as immune suppressants, antioxidants, antithrombosis, and anticoagulants.[9]

The atomic constitution of polyphenylbenzenes (only H and C) precludes the establishment of significant bond dipoles and local charge build ups. This fact, together with the relative size of these molecules, make dispersive interactions the more prominent ones in inter and intramolecular contacts. van der Waals interactions are the main component of the so-called aromatic interactions,[10,11] which also include a significant electrostatic contribution that confers some orientational preferences to aromatic complexes. Hence, these types of interactions can have a noticeable influence on the structure and stability of aromatic compounds, as for example polyphenylbenzenes.

The way phenyl substituents are distributed around the central benzene ring can induce some interesting structural changes at the supramolecular and molecular levels. These changes are reflected in thermodynamic differentiation, which can be easily perceived in the sublimation equilibrium and in gas phase

Received: August 8, 2011
Revised: September 11, 2011
Published: September 13, 2011

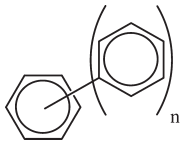

Figure 1. Schematic structure of the polyphenylbenzenes considered in this work ($n = 0-6$).

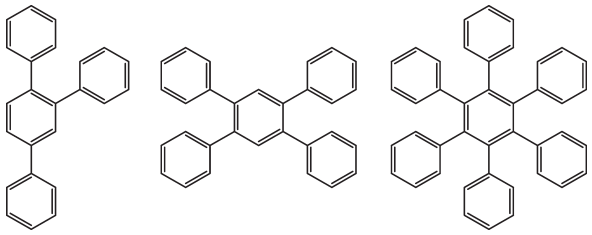

Figure 2. Schematic structure of the compounds studied in this work. From left to right: 1,2,4-triphenylbenzene (124tPhB), 1,2,4,5-tetraphenylbenzene (1245TPhB), and hexaphenylbenzene (HPhB).

energetics. In this work, special emphasis is given to the energetic/structural relationships in this family of compounds, focusing essentially in thermodynamic and X-ray crystallographic data. In this way, the literature data on polyphenylbenzenes was enriched by the measurement of the solid phase standard molar enthalpies of formation, $\Delta_f H^o_m(cr)$, by combustion calorimetry, and the derivation of the standard molar enthalpies, $\Delta^g_{cr} H^o_m$, and entropies, $\Delta^g_{cr} S^o_m$, of sublimation by a Knudsen/quartz crystal effusion technique, for the three polyphenylbenzenes illustrated in Figure 2. Gas phase standard molar enthalpies of formation, $\Delta_f H^o_m(g)$, were derived by the combination of the previous results. X-ray crystallography was used to determine molecular structure in the solid phase, whereas quantum chemistry was employed for the derivation of gas phase geometries, torsional profiles, and thermodynamic properties. In conjuction with the relevant literature data on this subject, a comprehensive thermodynamic and structural characterization of polyphenylbenzenes was made, emphasizing the observed structural/energetic relationships, and the origins of enthalpic and entropic differentiation.

The polyphenylbenzenes considered in this study are abbreviated as follows: *ortho*-terphenyl, *o*-dPhB; *meta*-terphenyl, *m*-dPhB; *para*-terphenyl, *p*-dPhB; 1,2,3-triphenylbenzene, 123tPhB; 1,2,4-triphenylbenzene, 124tPhB; 1,3,5-triphenylbenzene, 135tPhB; 1,2,4,5-tetraphenylbenzene, 1245TPhB; and hexaphenylbenzene, HPhB.

The properties of most chemical systems are a result of an entangled ensemble of physical−chemical effects that are hard to isolate and quantify individually. However, the nature and behavior of relatively simple chemical systems, like the polyphenylbenzenes studied in this work, are governed by a limited number of those effects, making their proper isolation, characterization, and quantification easier. Therefore, the systematic study of simple and interrelated compounds becomes of fundamental importance for the exploration and consolidation of chemical trends and laws.

2. EXPERIMENTAL SECTION

2.1. Synthesis, Purification, and Characterization of the Studied Compounds. Hexaphenylbenzene was commercially obtained from Sigma-Aldrich, washed with boiling acetone, and sublimed under reduced pressure. The compounds 1,2,4-triphenylbenzene and 1,2,4,5-tetraphenylbenzene were synthesized by the Suzuki-Miyaura cross-coupling methodology.[12,13]

1,2,4-Triphenylbenzene. A 150 mL solution of K_2CO_3 (120 mmol) in water was added to a solution of 1,2,4-tribromobenzene (15 mmol), phenylboronic acid (100 mmol), and palladium acetate (2 mol %) in 150 mL of DMF. The resultant solution was stirred at 90 °C for 9 h. The crude product was extracted with ethyl acetate. The organic phase was washed with water and NaOH(aq) 1 M and evaporated yielding a brown oil. A white solid began to precipitate with the addition of a few drops of ethanol (yield (%) = 81) The compound was purified by recrystallization with hexane and dichloromethane, and by sublimation under reduced pressure (mp = 118.8−120.4 °C).

1,2,4,5-Tetraphenylbenzene. A 160 mL solution of K_2CO_3 (140 mmol) in water was added to a solution of 1,2,4,5-tetrabromobenzene (15 mmol), phenylboronic acid (120 mmol), and palladium acetate (2 mol %) in 180 mL of DMF. The resultant solution was stirred at 90 °C for 9 h. The crude product was extracted with hot toluene and filtered over Celite. The resulting organic phase was washed with water and NaOH(aq) 1 M, and evaporated. The resulting precipitate was washed with ether and filtered yielding a white solid (yield (%) = 82). The compound was washed with boiling methanol and purified by sublimation under reduced pressure (mp = 272.8−274.3 °C). ^{1}H NMR (300 MHz, $CDCl_3$, 300 K, TMS): δ = 6.98 (s, 2H), δ = 6.96 (m, 20 H).

The identity of 124tPhB and 1245TPhB was confirmed by the X-ray crystal structures obtained and the purity of all the three compounds checked by gas chromatography, using an HP 4890 apparatus equipped with an HP-5 column, cross-linked, 5% diphenyl and 95% dimethylpolysiloxane, showing a %(m/m) purity greater than 99.9% in all cases.

2.2. Crystallographic Measurements. Crystal data, data acquisition conditions, and refinement parameters for 124tPhB and 1245TPhB are listed in the Supporting Information. Crystals of 124tPhB and 1245TPhB suitable for X-ray diffraction were obtained by slow evaporation from hexane and CH_2Cl_2 solutions, respectively. The intensity data was collected in a Bruker-Nonius CCD diffractometer. Data collection, cell refinement, and data reduction were made with the software package of the diffractometer: SMART[14] for data collection and SAINT[14] for cell refinement and for data reduction. Absorption correction was performed with SADABS.[15] The structures were solved and refined using the software: OSCAIL[16] and SHELXL97.[17] Molecular graphics were produced by ORTEPIII[18] and PLATON.[19] The complete set of structural parameters in CIF format is available as an Electronic Supplementary Publication from the Cambridge Crystallographic Data Centre (CCDC 736467 and 703163).

124tPhB crystallized in the orthorhombic system; space group *Pbca* from the systematic absences. 1245TPhB crystallized in the triclinic system; space group *P-1* assumed and confirmed by the analysis. The H atoms were treated as riding atoms with C−H(aromatic) = 0.95 Å with $U_{iso}(H) = 1.2U_{eq}(C)$.

2.3. Combustion Calorimetry. *1,2,4,5-Tetraphenylbenzene.* The standard molar enthalpy of combustion, $\Delta_c H^o_m$, at T = 298.15 K, was measured in an isoperibol static bomb combustion calorimeter with a twin valve bomb of internal volume of 0.290 dm^3, formerly used at the National Physical Laboratory, Teddington, U. K., and was used mainly as previously described, although a few changes in technique, due to different auxiliary equipment, were applied.[20,21]

Samples in pellet form were weighed in an analytical balance with a resolution of 0.01 mg and ignited in oxygen at a pressure of 3.04 MPa, with a volume of 1.00 cm^3 of water added to the bomb. From a weighed acrylic vessel, water was added to the calorimeter, and for each experiment a correction to the energy equivalent for the deviation from 2900.0 g of the mass of water added has been taken into account. Calorimetric temperatures were measured with a resolution of 1×10^{-5} K with an S10 four wire calibrated ultrastable thermistor (Thermometrics, standard serial No. 1030) and recorded by a 7 1/2 digits nano-ohm meter (Hewlett-Packard model 34420A), interfaced to a PC type computer, using the program LABTERMO v3.0.[22] Temperature measurements were automatically collected every 10 s and the initial temperature of the combustion experiments was very close to 298.15 K.

The energy equivalent of the calorimeter was determined from the combustion of benzoic acid (Calorimetric Standard NIST 39j), having a massic energy of combustion under bomb conditions of $-(26434.0 \pm 3.0)$ J g^{-1}, as previously described.[23] The electrical energy for the ignition was determined from the change in the potential difference across a 1400 μF condenser on discharge through a platinum ignition wire. For the cotton thread fuse (empirical formula $CH_{1.686}O_{0.843}$), the massic energy of combustion is assigned to $\Delta_c u^0 = -16240$ J g^{-1}.[24] Corrections for nitric acid formation were based on -59.7 kJ mol^{-1} for the molar energy of formation of 0.1 mol dm^{-3} HNO_3(aq) from O_2(g), N_2(g), and H_2O(l).[25] The amount of nitric acid was determined by titration against NaOH. During the combustion experiments, the sample purity, as well as combustion completeness was supported by a CO_2 recovery analysis. From 16 calibration experiments, the energy equivalent of the calorimeter, ε(calor)/(J K^{-1}), was found to be {15546.3 ± 1.8 (0.012%)} for an average mass of water added to the calorimeter of 2900.0 g; the quoted uncertainty refers to the standard deviation of the mean.

1,2,4-Triphenylbenzene and Hexaphenylbenzene. The standard molar enthalpies of combustion, $\Delta_c H^\circ_m$, at T = 298.15 K, were measured in an isoperibol mini-bomb combustion calorimeter.[26] The mini-bomb is made of stainless steel with 0.46 cm wall thickness and 18.185 cm^3 of internal volume. The internal fittings located on the head of the mini-bomb (electrodes, crucible support and sheet) are all made of platinum.

The samples were pressed in the form of pellets and placed in the platinum crucible, and their apparent mass weighed on a Mettler Toledo, model UMT2, microbalance with a sensitivity of $\pm 10^{-7}$ g. The electrical discharge for the ignition was made via a 2 cm long platinum wire (Goodfellow, mass fraction 0.999, Φ = 0.080 mm) tied in both electrodes terminals and bent down to a "V" shape toward the pellets. A platinum sheet with an inverted U shape was placed above the crucible assembly to concentrate the heat, thus helping to prevent the formation of carbon residues. Ultrapure water (0.050 cm^3) was added to the bomb before adjusting the head with an O-ring to the body of the mini-bomb by means of a retaining screw-ring. The bomb was purged four times and filled with ultrapure oxygen up to a pressure of 3.04 MPa. The bomb was then placed in its support, equipped with an electrical contact for electrical discharge, and introduced into the cylindrical copper block, which contains a bean type thermistor (R = 4 kΩ, at T = 298.15 K) for temperature measurement. Helium (mass fraction 0.9999) was used to fill the block up to 0.2 MPa, after purging, in order to improve heat conduction between the bomb and the block. The calorimetric system is surrounded by a thermostatic water bath, maintained at a constant temperature of 298.420 ± 0.001 K by a TRONAC temperature controller, model PTC-40. For data acquisition, a 6 1/2 digits multimeter (Keithley, model 2000) interfaced to a PC was used to measure the resistance of the thermistor every 10 s, in four-wire measurement mode. The charging, firing circuit, and voltage measurement across the 2000 μF discharger condenser are done automatically by means of a set of Advantech acquisition/automation modulus, series 4000. Real time recording and displaying of data is achieved with a modified version of the LABTERMO software.[22] The energy equivalent of the calorimeter, ε(calor)/J K^{-1} = 1945.77 ± 0.08 (0.004%), was obtained from a total of 36 calibration experiments, made with benzoic acid (Calorimetric Standard NIST 39j).

The amount of carbon soot, when formed, is determined gravimetrically, and this is considered for the total energy involved in the combustion process based on the value of $\Delta_c u^0$(C) = −33 kJ g^{-1}.[23] The densities of 124tPhB, 1245TPhB, and HPhB were taken from the crystallographic data presented in this work as 1.21, 1.25, and 1.17 g cm^{-3}, respectively. The values of $(\partial u/\partial p)_T$ at T = 298.15 K, were assumed to be −0.2 J g^{-1} MPa^{-1}.[27,28] The corresponding energetic correction usually leads to insignificant errors in the final combustion results. Standard state corrections were calculated for the initial and final states by the procedures given by Hubbard et al.[29] and by Good and Scott.[30] The relative atomic masses used were those recommended by the IUPAC Commission in 2005.[31]

2.4. Knudsen/Quartz Crystal Effusion. The vapor pressures of the three studied compounds as a function of temperature were measured by the combined Knudsen/quartz crystal effusion apparatus recently developed in our laboratory.[32] This technique is based on the simultaneous gravimetric and quartz crystal microbalance mass loss detection, enabling the use of a temperature-step methodology, and having the advantages of smaller sample sizes and effusion times and the possibility of achieving temperatures up to 650 K. For the measurement of pressures lower than 0.1 Pa a flow-concentrator device, placed between the oven and the quartz crystal, was used. Like a typical Knudsen effusion experiment, the system is kept at high vacuum, enabling free effusion of the vapor from the cell, and the oven is kept at a fixed temperature, T. During the effusion experiment, the rate of mass loss from the Knudsen effusion cell, dm(cell)/dt, is proportional to the rate of change of the mass deposited in the quartz crystal, dm/dt, as shown by eq 1

$$\frac{\mathrm{d}m(\mathrm{cell})}{\mathrm{d}t} = g\frac{\mathrm{d}m}{\mathrm{d}t} = g\frac{A_q}{S_q}\frac{\mathrm{d}f}{\mathrm{d}t} \quad (1)$$

where g is a geometric factor of the mass detection, A_q is the area of the quartz crystal, S_q is the mass sensitivity of the crystal, and df/dt is the rate of change of the resonance frequency of the quartz crystal. Taking $W = -S_q/(A_q g)$, where W is defined as the effective mass sensitivity coefficient, eq 1 becomes

$$\frac{\mathrm{d}f}{\mathrm{d}t} = -W\frac{\mathrm{d}m(\mathrm{cell})}{\mathrm{d}t} \quad (2)$$

To derive the vapor pressure, p, the value of W must be known for each compound. This value can be determined by weighing the total mass loss of the Knudsen cell, Δm(cell), during an independent experiment, and using eq 3

$$W = -\frac{\Delta f}{\Delta m(\mathrm{cell})} \quad (3)$$

where Δf is the total change in the crystal's resonance frequency in the whole experiment. The vapor pressures at each temperature are therefore obtained from eq 4

$$p = -\frac{df}{dt}\frac{1}{w_o A_o W}\left(\frac{2\pi RT}{M_M}\right)^{1/2} \quad (4)$$

where M_M is the molar mass of the effusing vapor, R is the gas constant, A_o is the area of the effusion orifice, and w_o is the transmission probability factor, which is usually calculated by means of eq 5, where l is the length of the effusion orifice and r its radius

$$w_o = \{1 + (3l/8r)\}^{-1} \quad (5)$$

In this technique only one effusion cell is used, with $l = 0.0125$ mm and $r = 0.500$ mm, giving $A_o = 0.7854$ mm^2 and $w_o = 0.9907$.

2.5. Calvet Microcalorimetry. The enthalpy change due to the heating of the sample in the crystalline phase from $T = 298.15$ K to the temperature T, $\{H^o_m(cr, T) - H^o_m(cr, 298.15\ K)\}$ was measured for each compound using a similar methodology to that described by Bernardes et al.[33] The values of $\Delta^T_{298.15K}H^o_m(cr)$ were determined for 124tPhB, 1245TPhB, and HPhB, using a high temperature Calvet microcalorimeter, SETARAM model HT1000D, described in the literature.[34] Samples of about 4−6 mg each were placed into thin capillary tubes, sealed at one end, and dropped simultaneously with the corresponding blank tube, at room temperature ($T = 298.15$ K), into the hot reaction zone of the calorimeter, at a fixed temperature, T.

From the previous results, the standard molar heat capacities of the crystalline phase, $C^o_{p,m}(T_m, cr)$ were derived for each compound, where T_m is the mean temperature between 298.15 K and the calorimeter hot zone temperature, T, which was very close to the mean temperature of the corresponding sublimation experiments, carried out in the Knudsen/quartz crystal apparatus. The microcalorimeter was calibrated with anthrancene at the respective temperature of the experiments for 124tPhB and with sapphire at the respective temperature of the experiments for 1245TPhB and HPhB. The calibration constants were found to be k(anthrancene, T_m = 331.8 K) = 0.9849 ± 0.0071, k(sapphire, T_m = 372.6 K) = 1.0099 ± 0.0007, and k(sapphire, T_m = 399.6 K) = 1.0068 ± 0.0064.

2.6. Computational Details. All theoretical calculations were performed using the Gaussian 03 software package.[35] The full geometry optimizations were performed using the Möller-Plesset perturbation theory with a second order perturbation (MP2) and the correlation consistent basis set cc-pVDZ, and density functional theory (DFT) with the hybrid exchange correlation functional (B3LYP) and the 6-311++G(d,p) basis set. The spin-component-scaled MP2 approach (SCS-MP2)[36] was also used for the calculation of electronic energies. The B3LYP/6-311++G(d,p) and MP2/cc-pVDZ levels of theory were used for frequencies calculations. The torsional potential profiles respecting the phenyl−phenyl (Ph-Ph) internal rotation in *ortho*-terphenyl ($\sigma_{int} = 2$) and *para*-terphenyl ($\sigma_{int} = 2$) were calculated at the MP2/cc-pVDZ level of theory, with full optimization of the remaining hyperspace potential. The contributions of these hindered rotors to $S^0(g)$ were estimated by a 1D hindered rotor analysis using the formalism introduced by Broadbelt and coworkers and the program CALCTHERM.[37−39] In this context the torsional potentials were fitted by a Fourier series, the hindered rotor Schrödinger equation solved numerically, and the thermodynamic quantities calculated accordingly.

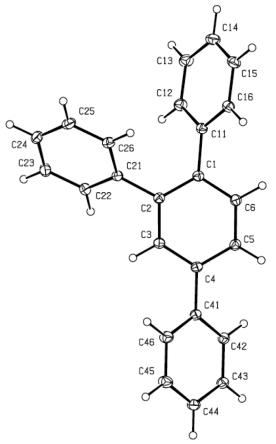

Figure 3. View of 124tPhB with our numbering scheme. Displacement ellipsoids are drawn at the 30% probability level.

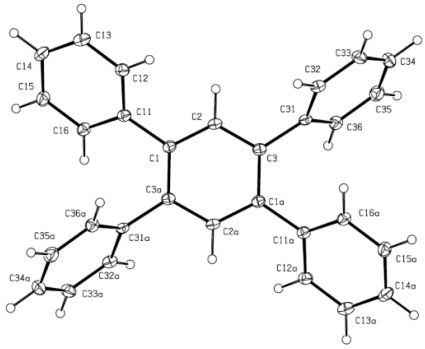

Figure 4. View of 1245TPhB with our numbering scheme. Displacement ellipsoids are drawn at the 30% probability level.

3. RESULTS

3.1. Structural Characterization. The X-ray structure determination for 124tPhB and 1245TPhB confirmed the expected molecular structures. A search made in the literature revealed that the crystalline structures for 1245TPhB,[40] and for HPhB[41] have been previously determined. Nevertheless the details of molecular conformation and supramolecular structures for these molecules were not presented by their authors, and so they will be discussed here. The molecular structure for 124tPhB is shown in Figure 3. The present data for 1245TPhB compares well with that of the structure previously published[40] which was collected at 93 K in spite of the fact that the present structure determination has a data completeness of 87% at $\theta = 25°$. The molecular structure for 1245TPhB is shown in Figure 4. The main bond lengths for the compounds are within the expected range for polyaromatics. The distances found for C−C bonds of the phenyl rings show values within the typical range of 1.384(13) corresponding to the mean value for the C_{ar}−C_{ar} bond in aromatic compounds.[42] Nevertheless, a systematic elongation of the C_{ar}−C_{ar} bonds on the central ring, which is more pronounced in HPhB, is observed. The dihedral angles between the mean planes of each of the phenyl rings with respect to the mean plane of the central benzene ring differ significantly between the studied compounds. The list of those angles is presented in Table 1.

Table 1. Dihedral Angles (°) between Mean Planes of Central Ring and Attached Rings

	dihedral angles/°		
attachment atom position[a]	124tPhB	1245TPhB[c]	HPhB
C1	50.66(5)	40.50(12)[b]	88.59(10)
C2	47.78(4)	65.96(12)[b]	75.53(10)
C3			87.95(12)
C4	42.03(5)	40.50(12)	82.17(11)
C5		65.96(12)	65.14(10)
C6			76.50(10)

[a] In the central ring. [b] For 1245TPhB C1 and C2 are centrosymetrically related to C4 and C5. [c] The corresponding values in ref 40 are 39.97(14)° and 66.01(14)°.

Table 2. Intermolecular Interactions (Å, °) in the Studied Compounds[a]

compound	D−H···A	H···A	D···A	D−A···A
124tPhB	C(22)−H(22)···π(1)^{i}	2.86	3.5378(10)	129
	C(43)−H(43)···π(11)^{ii}	2.90	3.7165(10)	145
	C(46)−H(46)···π(11)^{iii}	2.98	3.6653(10)	130
1245TPhB	C(14)−H(14)···π(31)^{iv}	2.78	3.636(3)	150
HPhB[b]	C(13)−H(13)···π(1)^{v}	2.85	3.782(3)	166
	C(43)−H(43)···π(1)^{vi}	2.80	3.699(3)	157

[a] π(31) is the centroid of the C31−C36 ring, π(1) is the centroid of the C1−C6 ring, and π(11) is the centroid of the C11−C16 ring. Symmetry codes: $i = 1 - x, 1 - y, 1 - z$; ii = $3/2 - x, 1 - y, -1/2 + z$; iii = $3/2 - x, -1/2 + y, z$; iv = $1 - x, -y, 1 - z$; v = $1/2 + x, 3/2 - y, z$; vi = $-1/2 + x, 1/2 - y, z$. [b] Atom labels corresponding to our numbering scheme.

Most phenyl dihedral angles in HPhB are at least 10° higher than those in 124tPhB and 1245TPhB. This can result from the steric hindrance imposed by neighboring substituents. It is interesting to note that, in each structure, the rings exhibiting lower dihedral angles are those participating in the C−H···π interactions involved in the supramolecular structures. These supramolecular structures are stabilized by weak C−H···π interactions: three in 124tPhB and two in 1245TPhB and HPhB. Their geometric parameters are summarized in Table 2 and the interactions are depicted in Figures 5−7.

3.2. Combustion Calorimetry. The detailed results for combustion calorimetry are presented in Supporting Information. The internal energy for the isothermal bomb process, ΔU_{IBP}, was calculated according to eq 6

$$\begin{aligned}\Delta U_{IBP} = & -\{\varepsilon(\text{calor}) \\ & + c_p(H_2O,l)\Delta m(H_2O)\}\Delta T_{ad} \\ & + (T_i - 298.15)\varepsilon_i \\ & + (298.15 - T_i - \Delta T_{ad})\varepsilon_f - \Delta U(\text{ign}) \end{aligned} \quad (6)$$

where $\Delta m(H_2O)$ is the deviation of the mass added to the calorimeter from 2900.0 g, the mass assigned to ε(calor), and ΔT_{ad} is the calorimeter adiabatic temperature change corrected for the heat exchange and the work of stirring, calculated with the LABTERMO program using the Regnault−Pfaundler method, and applying a second order fitting for the initial and final periods, as reported by Santos et al.[22] For the mini-bomb calorimeter $\Delta m(H_2O) = 0$ since the calorimetric fluid is helium instead of water. The meaning of all of the terms presented in eq 6 is explained in the Supporting Information. The products of combustion in the experiments consist of a gaseous phase and an aqueous mixture for which the thermodynamic properties are known. The values of $\Delta_c u^\circ$ refer to the reactions represented by eqs 7−9, for 124tPhB, 1245TPhB, and HPhB, respectively

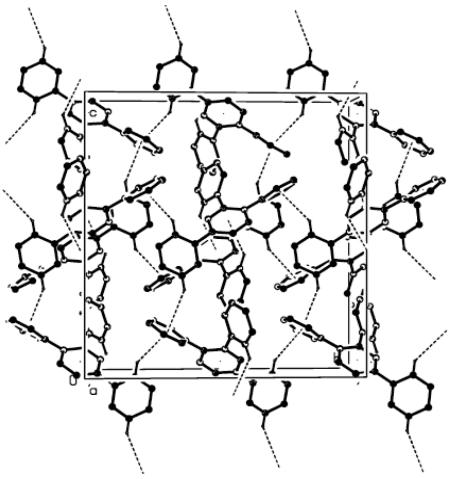

Figure 5. View of the supramolecular structure of 124tPhB, showing the C−H···π intermolecular interactions. Hydrogen atoms not involved in the motifs are not included.

$$C_{24}H_{18}(cr) + 57/2O_2(g) \rightarrow 24CO_2(g) + 9H_2O(l) \quad (7)$$

$$C_{30}H_{22}(cr) + 71/2O_2(g) \rightarrow 30CO_2(g) + 11H_2O(l) \quad (8)$$

$$C_{42}H_{30}(cr) + 99/2O_2(g) \rightarrow 42CO_2(g) + 15H_2O(l) \quad (9)$$

Table 3 lists the set of individual $\Delta_c u^\circ$ values obtained for each studied compound, as well as the mean $\Delta_c u^\circ$ and corresponding standard deviation of the mean. Table 4 lists the derived standard molar energies of combustion, $\Delta_c U^0_m(cr)$, the standard molar enthalpies of combustion, $\Delta_c H^0_m(cr)$, and the standard molar enthalpies of formation, $\Delta_f H^0_m(cr)$, of the crystalline solids. In accordance with the normal thermochemical practice, the uncertainties assigned to $\Delta_c H^0_m(cr)$ and $\Delta_f H^0_m(cr)$ are twice the overall standard deviation of the mean and include the uncertainties in calibration and in the auxiliary quantities used. To derive $\Delta_f H^0_m(cr)$ from $\Delta_c H^0_m(cr)$, the standard molar enthalpies of formation of $H_2O(l)$ and $CO_2(g)$ at $T = 298.15$ K, -285.830 ± 0.042 and -393.51 ± 0.13 kJ mol^{-1}, respectively, were used.[43]

3.3. Knudsen/Quartz Crystal Effusion. For the three compounds considered in this work, the standard molar enthalpies, $\Delta^g_{cr}H^\circ_m$, and entropies, $\Delta^g_{cr}S^\circ_m$, of sublimation at the mean temperature, $\langle T \rangle$, of the sublimation experiments were derived using the integrated form of the Clausius−Clapeyron equation

$$\ln p = a - b/T \quad (10)$$

where a is a constant and $b = \Delta^g_{cr}H_m(\langle T \rangle)/R$. Figure 8 presents a comparative plot of $\ln p = f(1/T)$ for the three studied compounds. The detailed sublimation results are given as

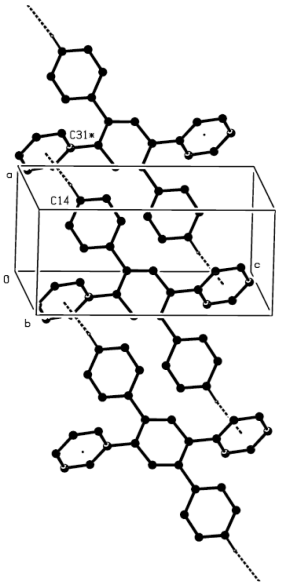

Figure 6. View of the supramolecular structure of 1245TPhB, showing the C−H···π intermolecular interactions. Hydrogen atoms not involved in the motifs are not included.

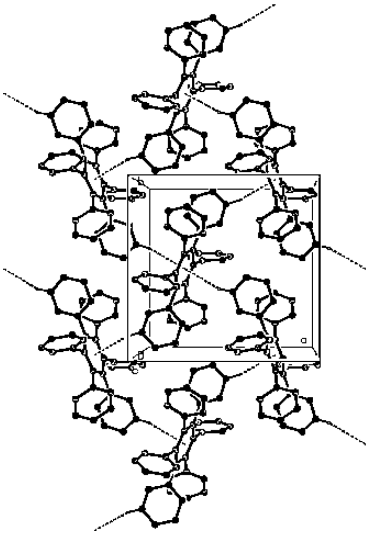

Figure 7. View of the supramolecular structure of HPhB, showing the C−H···π intermolecular interactions. Hydrogen atoms not involved in the motifs are not included.

Supporting Information. The values of $\Delta_{cr}^{g}H_m^{o}$ at $\langle T\rangle$ are determined by the parameter b of the Clausius−Clapeyron equation and the values of $\Delta_{cr}^{g}S_m$, at $p(\langle T\rangle)$ and at $\langle T\rangle$, $\Delta_{cr}^{g}S_m(\langle T\rangle, p(\langle T\rangle))$, are calculated as

$$\Delta_{cr}^{g}S_m(\langle T\rangle, p(\langle T\rangle)) = \Delta_{cr}^{g}H_m(\langle T\rangle)/\langle T\rangle \quad (11)$$

The standard molar enthalpies of sublimation, $\Delta_{cr}^{g}H_m^{o}$, at T = 298.15 K were determined by eq 12

$$\Delta_{cr}^{g}H_m^{o}(298.15\ \mathrm{K}) = \Delta_{cr}^{g}H_m(\langle T\rangle) + (298.15 - \langle T\rangle)\Delta_{cr}^{g}C_{p,m}^{0}(T_m) \quad (12)$$

Table 3. Individual Values of Standard Massic Energies of Combustion, $\Delta_c u^0$, for the Three Polyphenylbenzenes Studied, at T = 298.15 K[a]

124tPhB	1245TPhB	HPhB
	$\Delta_c u^o$/J g^{-1}	
−39976.93	−39855.82	−39859.00
−39983.03	−39871.87	−39884.59
−39971.66	−39852.69	−39864.89
−39972.94	−39864.78	−39861.96
−39975.38	−39860.52	−39863.20
−39981.19	−39870.12	−39875.18
−39974.03	−39862.04	−39861.41
−39980.77		−39866.63
		−39854.46
		−39869.96
	$\langle\Delta_c u^o\rangle$/J g^{-1}	
−39977.0 ± 1.5	−39862.5 ± 2.7	−39866.1 ± 2.7

[a] Error in $\langle\Delta_c u^0\rangle$ given as the standard deviation of the mean.

Table 4. Derived Standard Molar Energies of Combustion, $\Delta_c U_m^0$(cr), Standard Molar Enthalpies of Combustion, $\Delta_c H_m^0$(cr), and Standard Molar Enthalpies of Formation, $\Delta_f H_m^0$(cr), in the Crystalline State, at T = 298.15 K, for the Studied Compounds

	$\Delta_c U_m^0$(cr)/kJ mol^{-1}	$\Delta_c H_m^0$(cr)/kJ mol^{-1}	$\Delta_f H_m^0$(cr)/kJ mol^{-1}
124tPhB	−12249.2 ± 3.1	−12260.4 ± 3.1	243.6 ± 4.4
1245TPhB	−15247.6 ± 4.4	−15261.2 ± 4.4	311.8 ± 5.9
HPhB	−21316.4 ± 5.9	−21335.0 ± 5.9	520.1 ± 8.0

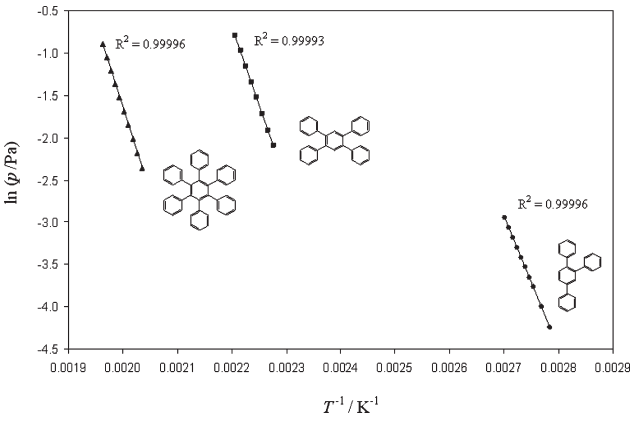

Figure 8. Plots of ln $p = f(1/T)$ for one experiment of each compound obtained by the Knudsen/quartz crystal effusion technique.

where $T_m = (\langle T\rangle + 298.15)/2$. The standard molar entropies of sublimation, $\Delta_{cr}^{g}S_m^{o}$, at T = 298.15 K, were calculated by the following equation:

$$\Delta_{cr}^{g}S_m^{o}(298.15\ \mathrm{K}) = \Delta_{cr}^{g}S_m(\langle T\rangle, p(\langle T\rangle)) + \Delta_{cr}^{g}C_{p,m}^{0}(T_m)\ln(298.15/\langle T\rangle) - R\ln(p^0/p(\langle T\rangle)) \quad (13)$$

where $p^o = 10^5$ Pa. The standard molar Gibbs energies of sublimation, $\Delta_{cr}^{g}G_m^{o}$, at T = 298.15 K, were calculated using

Table 5. Standard Molar Enthalpies, for the Crystalline Phase, from T = 298.15 K to the Temperature, T, Programmed in the Calvet Microcalorimeter, $\Delta^{T}_{298.15K}H^{o}_{m}$(cr), and the Derived $C^{o}_{p,m}(T_m, cr)$

	T/K	T_m/K	$\Delta^{T}_{298.15K}H^{o}_{m}$(cr)/kJ mol^{-1}	$C^{o}_{p,m}(T_m, cr)$/J K^{-1} mol^{-1}
124tPhB	365.43	331.8	26.9 ± 0.5	399.8 ± 7.8
1245TPhB	446.98	372.6	84.9 ± 1.3	570.4 ± 8.7
HPhB	500.99	399.6	166.0 ± 1.5	818.4 ± 8.6

Table 6. Standard Molar Enthalpies, Entropies and Gibbs Energies of Sublimation, at T = 298.15 K, for the Studied Compounds

	$\Delta^{g}_{cr}H^{0}_{m}$/kJ mol^{-1}	$\Delta^{g}_{cr}S^{0}_{m}$/J K^{-1} mol^{-1}	$\Delta^{g}_{cr}G^{0}_{m}$/kJ mol^{-1}
124tPhB	132.8 ± 0.7	239.7 ± 2.0	61.3 ± 0.9
1245TPhB	161.4 ± 1.6	257.5 ± 4.2	84.6 ± 2.0
HPhB	175.5 ± 2.1	245.4 ± 5.2	102.3 ± 2.6

eq 14

$$\Delta^{g}_{cr}G^{o}_{m}(298.15\ K) = \Delta^{g}_{cr}H^{o}_{m}(298.15\ K) - 298.15\Delta^{g}_{cr}S^{o}_{m}(298.15\ K) \quad (14)$$

The values of $\Delta^{g}_{cr}C^{0}_{p,m}$ (T_m), were calculated as

$$\Delta^{g}_{cr}C^{0}_{p,m}(T_m) = C^{o}_{p,m}(T_m, g) - C^{o}_{p,m}(T_m, cr) \quad (15)$$

The values of $C^{o}_{p,m}$ (T_m, g) were calculated by computational thermochemistry at the B3LYP/6-311++G(d,p) level of theory using the scaling factor of 0.9688[44] for the fundamental frequencies calculations: $C^{o}_{p,m}$(124tPhB, g) = 372.9 ± 5.0 J K^{-1} mol^{-1}, $C^{o}_{p,m}$(1245TPhB, g) = 523.2 ± 5.0 J K^{-1} mol^{-1}, and $C^{o}_{p,m}$(HPhB, g) = 781.9 ± 5.0 J K^{-1} mol^{-1} (the error of ±5.0 J K^{-1} mol^{-1} was assumed as an upper bound). The values of $C^{o}_{p,m}(T_m, cr)$ were derived from the values of $\Delta^{T}_{298.15K}H^{o}_{m}$(cr) measured by Calvet microcalorimetry. Table 5 lists the enthalpy change due to the heating of the sample in crystalline phase from T = 298.15 K to the programmed temperature, T, in the Calvet microcalorimeter and the derived $C^{o}_{p,m}(T_m, cr)$. Considering the values of $C^{o}_{p,m}(T_m, g)$ and $C^{o}_{p,m}(T_m, cr)$ obtained, the $\Delta^{g}_{cr}C^{o}_{p,m}(T_m)$ values were calculated as $\Delta^{g}_{cr}C^{o}_{p,m}$(124tPhB) = −26.9 ± 9.3 J K^{-1} mol^{-1}, $\Delta^{g}_{cr}C^{o}_{p,m}$(1245TPhB) = −47.2 ± 10.0 J K^{-1} mol^{-1}, and $\Delta^{g}_{cr}C^{o}_{p,m}$(HPhB) = −36.5 ± 9.9 J K^{-1} mol^{-1}. Table 6 lists the derived standard (p^o = 10^5 Pa) molar enthalpies, entropies and Gibbs energies of sublimation, at T = 298.15 K, for the three polyphenylbenzenes.

3.4. Computational Results. The results for the total electronic energies obtained from the optimized structures of the selected compounds, as well as the detailed results for the internal rotation torsional profiles are presented as Supporting Information. Figure 9 illustrates the three different hindered rotations considered in this work. The torsional profiles for the Ph-Ph torsion in *p*-dPhB (profile 1, P1), *o*-dPhB (profile 2, P2), and for the central phenyl substituent in 123tPhB (profile 3, P3), calculated at the MP2/cc-pVDZ level of theory, are presented in figure 10. The Ph-Ph torsional profile for *m*-dPhB is expected to be very similar to *p*-dPhB, as supported by the fact that a large resemblance in the profiles of *p*-dPhB (this work) and biphenyl,[45] is observed. For the central phenyl substituent of 123tPhB only the structure corresponding to the Ph-Ph dihedral of 0° (presumably the maximum) was calculated

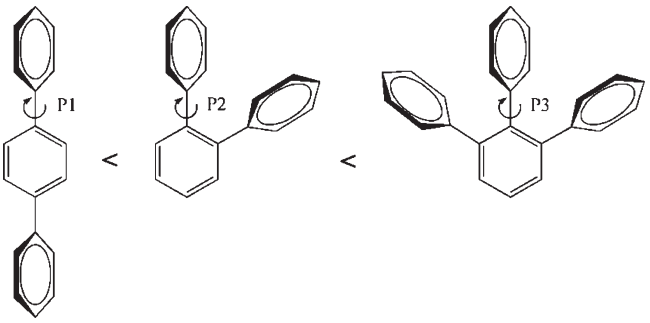

Figure 9. Three hindered rotations considered in this work. The associated barrier height increases in the order P1 < P2 < P3.

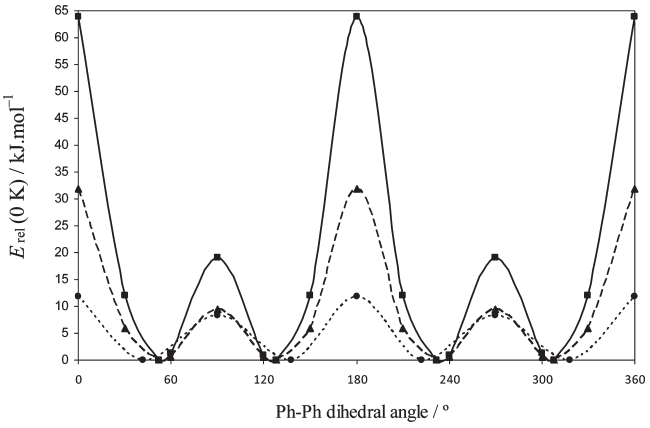

Figure 10. Potential energy profiles for the Ph-Ph torsion in *p*-dPhB (P1) (●), *o*-dPhB (P2) (▲), and the central phenyl substituent in 123tPhB (P3) (■), calculated at the MP2/cc-pVDZ level of theory.

and all the other points were scaled relative to the *o*-dPhB profile.

The above-mentioned profiles were used for the calculation of S^0(g), at T = 298.15 K, taking σ_{sym} = 1 for all cases, at the B3LYP/6-311++G(d,p) and MP2/cc-pVDZ levels of theory using, respectively, the scaling factors of 1.0161[44] and 0.9379[46] for entropy correction, and the program CALCTHERM.[37−39] The values of S^0(g) corrected for hindered rotation, considering the two Ph-Ph internal rotors in terphenyls, were calculated for *o*-dPhB (using P2), *m*-dPhB (using P1), *p*-dPhB (using P1) and an hypothetic *o*-dPhB (using P3) where the torsional profile obtained for the central Ph substituent in 123tPhB (P3) was used for describing the two Ph-Ph hindered rotations. These results are presented in table 7. Note that for very high rotational barriers, S^0(g) approaches the value derived within the harmonic oscillator (HO) approximation. Table 8 shows the derived hindered rotor entropy contributions, S^0_{HR}(g), associated to each hindered rotor profile considered in this work, P1, P2, and P3.

Table 7. Calculated $S^0(g)$, at T = 298.15, for *ortho*, *meta*, and *para*-Terphenyl, Taking into Account the Harmonic Oscillator (HO), P1, P2, and P3 Torsional Profiles, at the B3LYP/6-311++G(d,p) and MP2/cc-pVDZ Levels of Theory

		$S^0(g)$/J K^{-1} mol^{-1}	
molecule	torsional profile	MP2	B3LYP
o-dPhB	2 x HO	512.0	490.7
	2 x P2	523.7	503.1
	2 x P3	510.4	489.8
m-dPhB	2 x HO	514.4	492.2
	2 x P1	534.5	513.0
p-dPhB	2 x HO	514.6	493.3
	2 x P1	534.3	512.9

Table 8. Calculated Hindered Rotor Entropy Contributions, $S^0_{HR}(g)$, at T = 298.15 K, at the B3LYP/6-311++G(d,p) and MP2/cc-pVDZ Levels of Theory, Respecting the P1, P2, and P3 Hindered Rotor (HR) Profiles

	$S^0_{HR}(g)$/J K^{-1} mol^{-1}		
HR profile	MP2	B3LYP	mean
P1	28.6	28.6	28.6
P2	23.4	23.8	23.6
P3	16.8	17.2	17.0

Despite the discrepancy in individual values of $S^0(g)$ when comparing the B3LYP and MP2 methods, it is worth noting the very nice agreement in the $S^0_{HR}(g)$ values.

4. DISCUSSION

Table 9 lists the relevant thermodynamic quantities for polyphenylbenzenes. The standard molar enthalpies of formation in the gas phase, $\Delta_f H^0_m(g)$, at T = 298.15 K, for the studied compounds, were calculated according to eq 16

$$\Delta_f H^0_m(g, 298.15\ K) = \Delta_f H^0_m(cr, 298.15\ K) + \Delta^g_{cr} H^0_m(298.15\ K) \quad (16)$$

4.1. Sublimation Thermodynamics. *4.1.1. Contribution of Enthalpy.* In this series of compounds, the expected increse in $\Delta^g_{cr}H^0_m$, as the number of phenyl groups increases is observed. However, as illustrated in Figure 11, HPhB deviates considerably from the linear trend obtained by plotting $\Delta^g_{cr}H^0_m$ against the total number of phenyl substituents, n(Ph), for polyphenylbenzenes with at least one ortho relation. Another observation that can be drawn from Table 9 is that the compounds with ortho substituents tend to have lower $\Delta^g_{cr}H^0_m$, indicating a significant decrease of the cohesive energy as more surface area is buried from the intermolecular environment. This situation is driven to a limit in HPhB, where none of the phenyl substituents have free π-faces able to establish significant intermolecular interactions (dispersive and C−H···π), which results in the observed lower than expected $\Delta^g_{cr}H^0_m$. As mentioned in section 3.1 HPhB only establishes two C−H···π intermolecular interactions per molecule, a small number considering its molecular size.

Table 9. Selected Standard Molar Thermodynamic Quantities, at T = 298.15 K, for the Polyphenylbenzenes Considered in This Work

	n(Ph)[a]	$\Delta^g_{cr}H^0_m$/ kJ mol^{-1}	$\Delta^g_{cr}S^0_m$/ J K^{-1} mol^{-1}	$\Delta_f H^0_m(g)$/ kJ mol^{-1}
benzene[47,48]	0	44.7 ± 0.2[b]	140.6[b]	82.9 ± 0.9
biphenyl[49]	1	81.5 ± 0.2	180.3 ± 0.5	182.0 ± 0.7
o-dPhB[50]	2	103.0 ± 0.4	210.6 ± 1.3	285.5 ± 3.6
m-dPhB[50]	2	118.6 ± 0.7	233.1 ± 2.2	279.9 ± 3.9
p-dPhB[50]	2	125.6 ± 0.8	224.3 ± 2.2	284.4 ± 3.5
123tPhB[51]	3	134.1 ± 1.1	245.1 ± 3.2	376.7 ± 5.3
124tPhB	3	132.8 ± 0.7	239.7 ± 2.0	376.4 ± 4.5
135tPhB[51]	3	147.8 ± 0.7	254.0 ± 2.0	366.8 ± 4.9
1245TPhB	4	161.4 ± 1.6	257.5 ± 4.2	473.2 ± 6.1
HPhB	6	175.5 ± 2.1	245.4 ± 5.2	695.6 ± 8.3

[a] n(Ph) is the number of phenyl substituents in the benzene ring. [b] Derived hypothetical values: they refer to conditions of temperature and pressure at which benzene is a liquid.

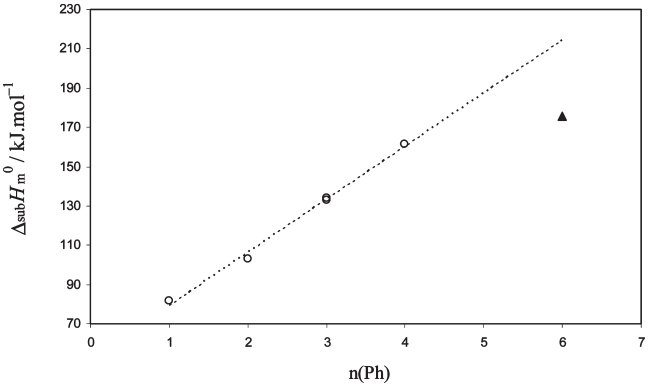

Figure 11. $\Delta^g_{cr}H^0_m$, at T = 298.15 K, as a function of the number of phenyl substituents in benzene, n(Ph), for the species with ortho related phenyl rings. HPhB is clearly an outlier.

4.1.2. Contribution of Entropy. A very poor correlation is observed between $\Delta^g_{cr}S^0_m$ and the number of phenyl substituents, n(Ph), as shown in Figure 12. Moreover, HPhB clearly has an abnormally low $\Delta^g_{cr}S^0_m$.

One factor that can impose some entropic differentiation is molecular symmetry. HPhB is a highly symmetric molecule belonging to the D_{6d} space group, which has associated an external symmetry number, σ_{sym}, of 12. The influence of molecular symmetry on entropy is still a matter of debate in the literature.[52−63] Strictly speaking, only entropy differences can be measured experimentally, and thus it is very hard to evaluate the real influence of molecular symmetry in the different phases of matter. In the case of entropies of sublimation, entropic differentiation due to symmetry can either be ascribed to a higher $S^0(cr)$, a lower $S^0(g)$, or a combination of both to varying extents. Quantitatively, the influence of symmetry on both phases is always on the direction of: higher symmetry → lower $\Delta^g_{cr}S^0_m$, by a factor that should be proportional to $R\ln(\sigma_{sym})$. However, these perspectives are fundamentally quite different. More symmetry leads to more ways of allocating the molecule in a given free space of the crystal lattice. In the condensation process the molecule strikes a structured lattice in a random orientation, and the

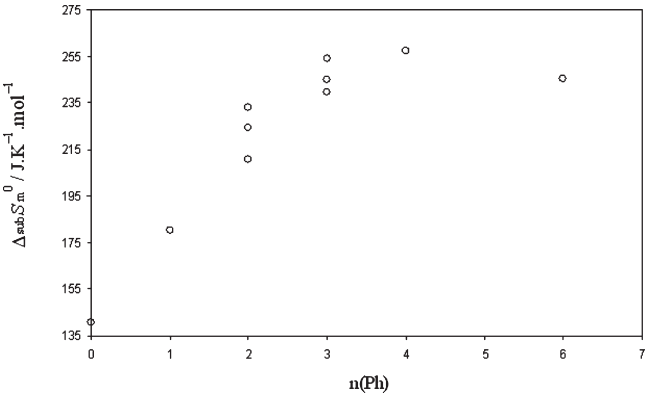

Figure 12. $\Delta_{cr}^{g}S_m^0$, at $T = 298.15$ K, as a function of the number of phenyl substituents in benzene, n(Ph).

probability of effectively condensing or bouncing off is affected by that orientation. A molecule will crystallize more easily if it strikes the solid surface with the orientation that it will adopt in that specific point of the crystal lattice. Symmetry increases the likelihood of a successful strike by increasing the number of correct molecular orientations, in an analogous way that geometric factors influence reaction kinetics. Put it simply, higher molecular symmetry should increase the sticking coefficient in the condensation process. Hence, higher symmetry can be associated with a faster condensation process, contributing for a lower volatility. This can be understood thermodynamically in terms of the so-called concept of residual entropy, which is a nonthermal contribution to S^0(cr), and arises because symmetry increases the number of equivalent ways into which the crystal phase can be realized. This is so because in the crystal phase each molecule and atom can be considered distinguishable since a specific and unique set of geometrical coordinates can be ascribed to each of them, irrespective of their identity.[64,65] On the other hand, σ_{sym} is introduced in the expression for the rotational molecular partition function in order to correct for an overcounting of the microscopically indistinguishable rotational states that are not allowed by the Pauli exclusion principle in a symmetric molecule. This arises from the parity restrictions of the molecular wave function for fermions, which must be antisymmetric with respect to the interchange of identical nuclei in the molecule.[66,67] In this way higher symmetry can also lead to a decrease of S^0(g). The real situation should follow the following reasoning: in the crystal phase more symmetry leads to a larger number of allowed permutations of the atoms compatible with a given macrostate (higher S^0(cr)), whereas in gas phase some of those permutations are forbidden by quantum mechanical requirements (lower S^0(g)) when the molecules do not possess ways so as to render those requirements less important. For instance, the polyphenylbenzenes studied in this work are relatively big and flexible molecules, and hence rotational−vibrational coupling may easily occur and partially or fully compensate for the entropic penalty associated to symmetry in the gas phase. For each compound considered in this work, σ_{sym}, corresponding to the number of unique orientations of the rigid molecule that only interchange identical atoms, was taken from the analysis of the X-ray crystal structures, contained in this work and in the literature. This was done approaching the observed solid phase structure to the molecular geometry that corresponds to the closest point group with highest symmetry. Since it is considered in this work that symmetry may affect both S^0(cr) and S^0(g) its influence on $\Delta_{cr}^{g}S_m^0$ shall be more correctly described as $cR\ln(\sigma_{sym})$, where c is a factor of proportionality.

Another origin of entropic differentiation in these compounds is the vibrational freedom of the phenyl substituents, with respect to the phenyl−phenyl torsion. The three hindered rotations illustrated in figure 9 can be clearly distinguished: the phenyl substituent with no ortho neighbors (e.g., the two phenyls in *p*-dPhB), one ortho neighbor (e.g., the two phenyls in *o*-dPhB) and two ortho neighbors (e.g., the central phenyl substituent in 123tPhB). It was expected, on the basis of simple stereochemistry, and verified computationally (figure 10) that the barrier height increases in the direction of 0, 1, and 2 ortho neighbors. A higher rotational barrier implies a more hindered torsional motion, and thus an associated decrease in vibrational entropy, as can be inferred from table 8. This differentiation will be predominantly noted in the gas phase, since in the crystal lattice these high-amplitude vibrational modes are much more restricted due to molecular packing. This can be pictured in the sublimation process as a number of frozen torsional modes in the crystalline state becoming free to rotate in the gas phase to different extents, depending on the number of ortho neighbors. In this perspective, a phenyl with no ortho neighbors will be freed to a higher extent than one with two ortho neighbors, resulting in a more pronounced increase in entropy for the former, and consequently raising $\Delta_{cr}^{g}S_m^0$ relative to the latter. This contribution in polyphenylbenzenes can be quantified based on the calculated P1, P2, and P3 hindered rotor profiles shown in Figures 9 and 10, and the respective hindered rotor entropies, S_{HR}^0(g), presented in Table 8. The following assumptions were made:

1- The 1D hindered rotor profiles for each phenyl substituent in polyphenylbenzenes have an additive contribution to S^0(g) and are based on the ones calculated for *o*-dPhB and *p*-dPhB, namely P1, P2, and P3.
2- Meta substituents were treated as para substituents, since S^0(*m*-dPhB, g) ≈ S^0(*p*-dPhB, g), as shown in Table 7, and the corresponding torsional profiles should be very alike.

The previous considerations about symmetry and hindered rotation suggest that an additive estimation model for $\Delta_{cr}^{g}S_m^0$ can be employed in this class of compounds. This model takes symmetry and hindered rotation into account and can be mathematically described by eq 17

$$\begin{aligned}\Delta_{cr}^{g}S_m^0(\text{model}) = {} & a + bn(\text{Ph}) - cR\ln(\sigma_{sym}) \\ & + S_{HR}^0(\text{g, P1})n(m/p\text{-Ph}) \\ & + S_{HR}^0(\text{g, P2})n(o\text{-Ph}) \\ & + S_{HR}^0(\text{g, P3})n(\text{central-Ph}) \end{aligned} \quad (17)$$

where a, b, and c are fitting parameters, n(Ph) is the total number of phenyl substituents relative to the central benzene ring, and $n(m/p\text{-Ph})$, $n(o\text{-Ph})$, and n(central-Ph) are respectively the number of phenyl rings with 0, 1, and 2 ortho relations in a given molecule. The values of S_{HR}^0(g,P1), S_{HR}^0(g,P2), and S_{HR}^0(g,P3) were taken as the mean values presented in Table 8. Increased symmetry will increase S^0(cr) and/or lower S^0(g), thus, decreasing $\Delta_{cr}^{g}S_m^0$, hence the "−" sign in the respective term. Less hindered rotations will increase S^0(g), thus increasing $\Delta_{cr}^{g}S_m^0$, hence, the "+" sign in the corresponding terms.

For each polyphenylbenzene studied in this work, Table 10 presents the molecular symmetry point group and the corresponding σ_{sym}, and the number of phenyl groups with 0, 1, and 2 ortho neighbors, $n(m/p\text{-Ph})$, $n(o\text{-Ph})$, and n(central-Ph), respectively.

Table 10. Molecular Symmetry Point Group and Associated External Symmetry Number, σ_{sym}, and the Number of Phenyl Groups with 0, 1, and 2 ortho Relations, $n(m/p\text{-Ph})$, $n(o\text{-Ph})$, and n(central-Ph), Respectively, for Each Studied Polyphenylbenzene

	point group	σ_{sym}	$n(m/p\text{-Ph})$	$n(o\text{-Ph})$	n(central-Ph)
benzene[68]	D_{6h}	12	0	0	0
bBiphenyl[69]	D_2	4	1	0	0
o-dPhB[70]	C_2	2	0	2	0
m-dPhB[71]	C_s	1	2	0	0
p-dPhB[72]	C_{2h}	2	2	0	0
123tPhB	C_2	2	0	2	1
124tPhB	C_1	1	1	2	0
135tPhB[73]	C_2	2	3	0	0
1245TPhB	C_{2h}	2	0	4	0
HPhB[41]	D_{6d}	12	0	0	6

The references of the X-ray crystallographic structures used to determine the symmetry point groups are shown near the compound's name.

By the least-squares method the values for the fitting parameters in eq 17 are a = 171.1 J K^{-1} mol^{-1}, b = 0.3 J K^{-1} mol^{-1}, and c = 1.4, giving an average error between the experimental and estimated $\Delta_{cr}^{g}S_m^0$ values of 2.8 J K^{-1} mol^{-1}, which corresponds approximately to 1% deviation (since 123tPhB was found to be an outsider it was not included in the fitting). The contributions for $\Delta_{cr}^{g}S_m^0$ considered within this model are schematically represented in Figure 13.

In this figure the $\Delta_{cr}^{g}S_m^0$ term on the left corresponds to the hypothetical situation were entropic differentiation is only due to the number of Ph substituents. The other two terms (symmetry and hindered rotation) are then considered in order to reproduce the experimental $\Delta_{cr}^{g}S_m^0$ values by the present model. It is interesting to note that $b \approx 0$ in eq 17, which can indicate that virtually no entropic differentiation would be observed if only the molar mass was considered. In this case, $\Delta_{cr}^{g}S_m^0$ could be chiefly ascribed to the translational and rotational (neglecting symmetry considerations) contributions, which have a smaller dependency on molar mass. The fact that c = 1.4 suggests that symmetry influences both S^0(cr) and S^0(g) to varying extents. This also suggests that symmetry shall not be fully active in differentiating entropically both phases, since c < 2. A partial influence of symmetry on entropy can be understood in terms of continuous symmetry numbers, as stated by other authors.[54,63] Since internal dynamics causes the molecules to incessantly interconvert between many more or less symmetric, transient and equilibrium structures, a fractional symmetry number seems more adequate to describe the real average situation, particularly when considering compounds with high molecular flexibility like most polyphenylbenzenes studied in this work. The value of c in eq 17 translates the average contribution of symmetry concerning all the compounds included in the fitting and is not necessarily the same for all of them, given, for instance, the different degree to which each molecule can distort from its equilibrium structure.

Figure 14 plots the values of $\Delta_{cr}^{g}S_m^0$(model) versus the experimental values of $\Delta_{cr}^{g}S_m^0$ for the polyphenylbenzenes studied in this work.

The good agreement obtained is a strong indication that molecular symmetry and the vibrational entropy associated with

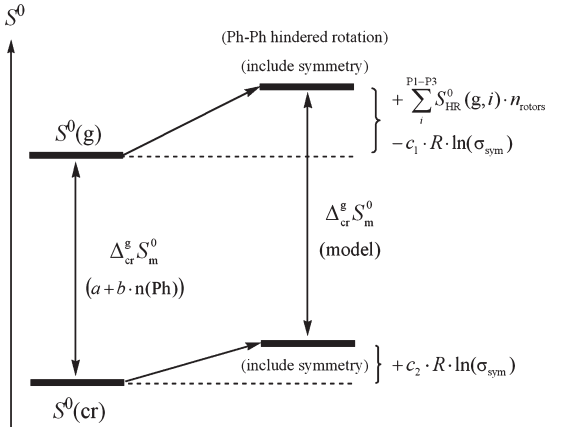

Figure 13. Schematic representation of the model used in this work for the calculation of $\Delta_{cr}^{g}S_m^0$, at T = 298.15 K, in polyphenylbenzenes, $c_1 + c_2 = c$ (in eq 17).

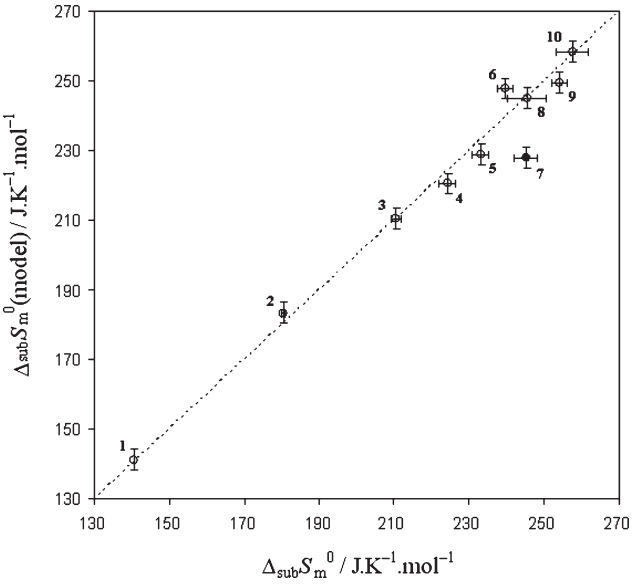

Figure 14. Plot of $\Delta_{cr}^{g}S_m^0$(model) versus the experimental values of $\Delta_{cr}^{g}S_m^0$ for the studied polyphenylbenzenes, at T = 298.15 K. 123tPhB (**7**), was not considered in the fitting. An average error of ±3 J K^{-1} mol^{-1} was considered for $\Delta_{cr}^{g}S_m^0$(model). Legend: benzene (**1**), biphenyl (**2**), *o*-dPhB (**3**), *p*-dPhB (**4**), *m*-dPhB (**5**), 124tPhB (**6**), 123tPhB (**7**), HPhB (**8**), 135tPhB (**9**), and 1245TPhB (**10**).

the Ph-Ph hindered rotations in this class of compounds are key factors influencing the differentiation in $\Delta_{cr}^{g}S_m^0$, with higher symmetry and a more pronounced hindered phenyl internal rotation contributing for a decrease of $\Delta_{cr}^{g}S_m^0$.

From Figure 14 one can see that 123tPhB presents a low $\Delta_{cr}^{g}S_m^0$(model). From the rationale presented thus far one can conclude that the model described by eq 17 should include at least one additional positive term respecting this compound. This indicates that in 123tPhB some unknown factor is increasing $\Delta_{cr}^{g}S_m^0$, either by decreasing S^0(cr) or increasing S^0(g). Unfortunately, despite of the efforts, we could not obtain suitable crystals for X-ray diffraction, and no crystal structure was found in the literature. A lower thermodynamic stability of the solid phase (which can derive from a lower S^0(cr)) could explain the

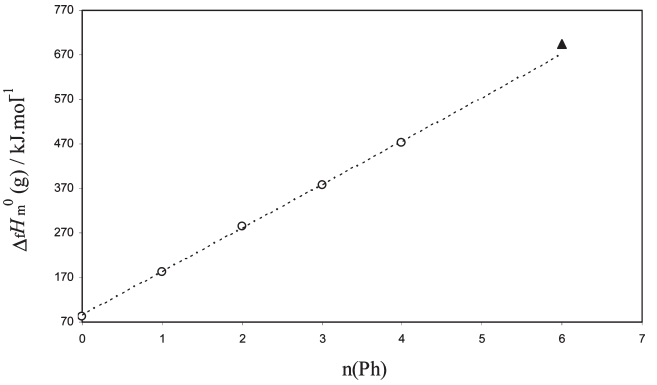

Figure 15. $\Delta_f H_m^0(g)$, at T = 298.15 K, as a function of the number of phenyl substituents in benzene, n(Ph), for the species with ortho-related phenyl rings. HPhB is an outlier.

difficulties in the crystallization process. However, this is not reflected in the melting points of the triphenylbenzene isomers: m.p.(123tPhB) ≈ 158 °C, m.p.(124tPhB) ≈ 120 °C, and m.p.(135tPhB) ≈ 173 °C. In principle, a significant decrease in S^0(cr) should lead to a considerably lower melting point of 123tPhB relative to its isomers. In gas phase, the most obvious explanation for an increased S^0(g) of 123tPhB is an ill description of the vibrational motions, including internal rotations. Substantial vibrational coupling may occur and free the Ph-Ph hindered rotations to some extent, thus raising S^0(g).

4.2. Gas Phase Energetics. A linear trend was obtained when ploting $\Delta_f H_m^0(g)$ versus the number of phenyl substituents, n(Ph), for polyphenylbenzenes with at least one ortho relation, as depicted in Figure 15.

HPhB is an outlier in the correlation, showing a marked increase in $\Delta_f H_m^0(g)$, which is associated with some additional destabilization in this molecule. The homodesmotic reaction presented in Figure 16, concerning the breaking of the phenyl−phenyl bonds in the polyphenylbenzenes to yield only biphenyls, is a good way to measure the total interaction enthalpy between the phenyl substituents in a given polyphenylbenzene. When $\Delta_{HR}H_m^o(g) < 0$, this interaction has an enthalpic destabilizing effect, and when $\Delta_{HR}H_m^o(g) > 0$, it has a stabilizing effect. The computational and experimental results obtained for $\Delta_{HR}H_m^o(g)$ are presented in Table 11.

The values of $\Delta_f H_m^0$(cr) for all of the compounds presented in Table 9 were determined by combustion calorimetry. Thus, in the calculation of the uncertainties in $\Delta_{HR}H_m^o(g)$, the contributions of the uncertainties of $CO_2(g)$ and $H_2O(l)$ in the overall uncertainties cancel out, and can be ignored. It was assumed that $\Delta_{HR}E_{el,m} \approx \Delta_{HR}H_m^o$(g, 298.15 K), where $\Delta_{HR}E_{el,m}$ is the molar energy of the homodesmotic reaction derived using the values of E_{el}(0 K) for each species, calculated by B3LYP/6-311++G(d,p) and SCS-MP2/cc-pVDZ. The corrections to ZPE and thermal enthalpy were neglected since they are generally of little significance in an homodesmotic approach.

Despite the fact that all of the studied compounds are aromatic, aromaticity is not expected to be an important source of energetic differentiation among them, since there are no apparent reasons for aromaticity to be significantly enhanced or disrupted in any of these molecules. The five main observations that can be drawn from the results obtained are the following:

1. $\Delta_{HR}H_m^o(g)$ tends to be more positive as more phenyl substituents are present, indicating the existence of some sort of through-space stabilizing interaction in these molecules. The fact that for 135tPhB the DFT result is more negative than the MP2 one may indicate that correlation energy is a source of stabilization in this molecule.
2. Meta relations have a more pronounced stabilizing effect.
3. The intramolecular interactions between ortho-related phenyl rings are significantly overestimated by DFT in the direction of increased steric repulsion. In reality, the existence of ortho substituents does not have such a noteworthy destabilizing effect, possibly indicating the existence of a considerable van der Waals attractive term (which would be ill described by B3LYP), characteristic of an intramolecular $\pi\cdots\pi$ interaction between the two adjacent phenyl rings.
4. In general SCS-MP2 accounts well for the energetics of gaseous polyphenylbenzenes, with higher deviations being observed for bigger molecules.
5. HPhB clearly has an additional destabilizing effect, possibly related to the fact that the phenyl substituents do not possess the ability to relieve strain by increasing the distance between the ortho groups. This can be achieved in the other polyphenylbenzenes with ortho relations, where the molecular compactness is not enough to restrain a geometrical relaxation. This fact is supported by the X-ray crystal structures for the studied polyphenylbenzenes. Like mentioned in section 3.1, the Ph-Ph dihedral angles in HPhB tend to be higher, which may be related with enhanced steric hindrance. As well a more pronounced elongation of the $C_{ar}-C_{ar}$ bonds in the central ring is observed. The C−C−C angle, α_{CCC}, schematized in Figure 17, is about 120° for phenyl rings with no ortho relation (e.g., 135tPhB), slightly higher, ∼123°, for *ortho*-phenyls (e.g., 1245TPhB), and ∼120° in HPhB. For HPhB the centroid-centroid distance between two *ortho*-phenyls,

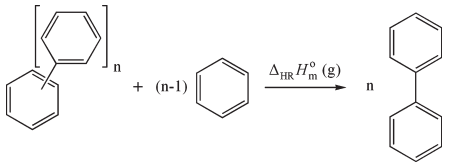

Figure 16. General homodesmotic reaction scheme used for the evaluation of the total substituent interaction enthalpy in polyphenylbenzenes.

Table 11. Experimental and Calculated (B3LYP/6-311++G(d,p) and SCS-MP2) Values of $\Delta_{HR}H_m^o(g)$, at T = 298.15 K, for the Individual Homodesmotic Reactions Presented in Figure 16

	$\Delta_{HR}H_m^o(g)$/kJ mol^{-1}		
	DFT	SCS-MP2	exp.
o-dPhB	−15.4	−0.9	−4.4 ± 3.0
m-dPhB	−0.6	1.2	1.2 ± 3.4
p-dPhB	0.4	1.1	−3.3 ± 2.9
123tPhB	−33.2	−1.3	3.5 ± 4.6
124tPhB	−15.2	1.4	3.8 ± 3.6
135tPhB	−1.2	3.7	13.4 ± 4.1
1245TPhB	−30.7	2.7	6.1 ± 5.1
HPhB			−18.1 ± 6.7

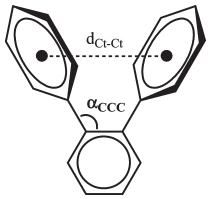

Figure 17. Relevant geometrical parameters in the crystalline state, obtained by X-ray crystallography, for a general polyphenylbenzene with an ortho relation.

$d_{Ct\text{-}Ct}$, is about 4.3 Å, whereas for the other *ortho*-polyphenylbenzenes it is ~4.7 Å. These facts indicate that ortho rings tend to relieve some strain by increasing α_{CCC}, and that this cannot be achieved in HPhB, due to its molecular compactness. Because this phenomenon is multiplied by six in HPhB, a substantial increase in $\Delta_f H^0_m(g)$ is observed.

Recently, an interesting review paper concerning twisted acenes presented a survey on their structures and properties.[74] Twisted acenes are compounds with unusual geometries, and some of them are structurally related to polyphenylbenzenes, particularly with HPhB. However, the X-ray and computationally optimized geometries of the polyphenylbenzenes studied in this work do not show any significant geometry twisting, and thus, this interesting phenomenon needs not be considered for the rationalization of structure and energetics in this case.

5. CONCLUSIONS

In this work, an experimental approach comprising combustion calorimetry and Knudsen/quartz crystal effusion was used for the derivation of the relevant thermodynamic quantities for 124tPhB, 1245TPhB, and HPhB. The crystal structures for 124tPhB and 1245TPhB were obtained by X-ray crystallography. These results, together with the data available in the literature for polyphenylbenzenes, provided some important insights into the structural/energetic relationships and the origins of enthalpic and entropic differentiation in this family of compounds. A parallel computational approach was used as a support of the experimetal results. It was observed that cohesive forces in the crystal phase are substantially reduced by the presence of ortho-related phenyl substituents, HPhB being an extreme case, due to the diminished molecular surface area able to establish intermolecular interactions. It was found that the observed trend in $\Delta^g_{cr}S^0_m$ for this series of compounds can be adequately reproduced when the influences of molecular symmetry and the different hindered rotor profiles of phenyl substituents in the sublimation equilibrium are considered. This is a good indication that the differentiation in the entropy of sublimation in polyphenylbenzenes is largely determined by these two factors: higher symmetry and more hindered Ph-Ph internal rotation contribute to a decrease of $\Delta^g_{cr}S^0_m$. This observation may also be extended to other molecular systems, suggesting that molecular symmetry and the degree of hindered internal rotation are important sources of entropic differentiation. The molecular compactness of HPhB prevents the relieve of strain due to phenyl−phenyl steric crowding, leading to a significant enthalpic destabilization in the gas phase.

■ ASSOCIATED CONTENT

Ⓢ Supporting Information. Detailed crystal data, combustion results, and vapor pressure data for 123tPhB, 1245TPhB, and HPhB, computational data, and optimized geometries. This material is available free of charge via the Internet at http://pubs.acs.org.

■ AUTHOR INFORMATION

Corresponding Author

*Fax: +351 220402659. Fax: +351 220402836. E-mail: lbsantos@fc.up.pt.

■ ACKNOWLEDGMENT

Thanks are due to Fundação para a Ciência e Tecnologia (FCT) and Programa Operacional Ciência e Inovação 2010 (POCI 2010) supported by the European Community Fund FEDER for the financial support to Project POCI/QUI/61873/2004. C.F.R.A.C.L. and M.A.A.R. also thank FCT and the European Social Fund (ESF) under the third Community Support Framework (CSF) for the award of Ph.D. Research Grants SFRH/BD/29394/2006 and SFRH/BD/60513/2009, respectively.

■ REFERENCES

(1) Kudchadkar, S. R.; Wiest, J. M. *J. Chem. Phys.* **1995**, *103*, 8566–8576.
(2) Robinson, T.; Kispert, L. D.; Joseph, J. *J. Chem. Phys.* **1985**, *82*, 1539–1542.
(3) Burroughes, J. H.; Bradley, D. D. C.; Brown, A. R.; Marks, R. N.; Mackay, K.; Friend, R. H.; Burn, P. L.; Holmes, A. B. *Nature* **1990**, *347*, 539–541.
(4) Grem, G.; Leditzky, G.; Ullrich, B.; Leising, G. *Adv. Mater.* **1992**, *4*, 36–37.
(5) Furumoto, H. W.; Ceccon, H. L. *J. Quantum Electron.* **1970**, *QE-6*, 262–268.
(6) Schmidt, J. A. R.; Arnold, J. *Organomtallics* **2002**, *21*, 2306–2313.
(7) Dickie, D. A.; Jalali, H.; Samant, R. G.; Jennings, M. C.; Clyburne, J. A. C. *Can. J. Chem.* **2004**, *82*, 1346–1352.
(8) Lee, D.; Hung, P. L.; Spingler, B.; Lippard, S. J. *Inorg. Chem.* **2002**, *41*, 521–531.
(9) Liu, J. K. *Chem. Rev.* **2006**, *106*, 2209–2223.
(10) Hunter, C. A.; Lawson, K. R.; Perkins, J.; Urch, C. J. *J. Chem. Soc., Perkin Trans. 2* **2001**, 651–669.
(11) Sinnokrot, M. O.; Sherrill, C. D. *J. Phys. Chem. A* **2006**, *110*, 10656–10668.
(12) Miyaura, N.; Yanagi, T.; Suzuki, A. *Synth. Commun.* **1981**, *11* (7), 513–519.
(13) Miyaura, N.; Suzuki, A. *Chem. Rev.* **1995**, *95*, 2457–2483.
(14) Bruker; Smart APEX (version 5.62), SAINT (Version 6.02), SHELXTL (Version 6.10) and SADABS (Version 2.03). Bruker AXS Inc.: Madison, WI, 2004.
(15) Sheldrick, G. M.; SADABS − Bruker Nonius area detector scaling and absorption correction − V2.10, 2003.
(16) McArdle, P.; Gilligan, K.; Cunningham, D.; Dark, R.; Mahon, M. *CrystEngComm* **2004**, *6*, 303–309.
(17) Sheldrick, G. M.; SHELXS97 and SHELXL97. Program for Crystal Structure Refinement; University of Göttingen: Göttingen, Germany, 1997.
(18) Johnson, C. K.; Burnett, M. N.; ORTEPIII for Windows; University of Glasgow: Glasgow, U.K., 1998.
(19) Spek, A. L. *J. Appl. Crystallogr.* **2003**, *36*, 7–13.
(20) Gundry, H. A.; Harrop, D.; Head, A. J.; Lewis, G. B. *J. Chem. Thermodyn.* **1969**, *1*, 321–332.
(21) Bickerton, J.; Pilcher, G.; Al-Takhin, G. *J. Chem. Thermodyn.* **1984**, *16*, 373–378.
(22) Santos, L. M. N. B. F.; Silva, M. T.; Schröder, B.; Gomes, L. *J. Therm. Anal. Calorim.* **2007**, *89*, 175–180.

(23) Coops, J.; Jessup, R. S.; van Nes, K. G. In *Experimental Thermochemistry*; Rossini, F. D., Ed.; Interscience: New York, 1956; Vol. 1, Chapter 3.
(24) Good, W. D.; Scott, D. W.; Waddington, G. *J. Phys. Chem.* **1956**, *60*, 1080–1089.
(25) Wagman, D. D.; Evans, W. H.; Parker, V. B.; Schumm, R. H.; Halow, I.; Bailey, S. M.; Churney, K. L.; Nuttall, R. L. *J. Phys. Chem. Ref. Data* **1982**, *11*, Suppl. 2.
(26) Ribeiro da Silva, M. A. V.; Pilcher, G.; Santos, L. M. N. B. F.; Lima, L. M. S. S. *J. Chem. Thermodyn.* **2007**, *39*, 689–697.
(27) Johnson, W. H. *J. Res. Natl. Bur. Stand.* **1975**, *79A*, 425–429.
(28) Washburn, E. W. *J. Res. Natl. Bur. Stand.* **1933**, *10*, 525–558.
(29) Hubbard, W. N.; Scott, D. W.; Waddington, G. In *Experimental Thermochemistry*; Rossini, F. D., Ed.; Interscience: New York, 1956; Vol. 1, Chapter 5.
(30) Good, W. D.; Scott, D. W. In *Experimental Thermochemistry*; Skinner, H. A., Ed.; Interscience: New York, 1962; Vol. 2, Chapter 2.
(31) Wieser, M. E. *Pure Appl. Chem.* **2006**, *78*, 2051–2066.
(32) Santos, L. M. N. B. F.; Lima, L. M. S. S.; Lima, C. F. R. A. C.; Magalhães, F. D.; Torres, M. C.; Schröder, B.; Ribeiro da Silva, M. A. V. *J. Chem. Thermodyn.* **2011**, *43*, 834–843.
(33) Bernardes, C. E. S.; Santos, L. M. N. B. F.; Minas da Piedade, M. E. *Meas. Sci. Technol.* **2006**, *17*, 1405–1408.
(34) Santos, L. M. N. B. F.; Schröder, B.; Fernandes, O. O. P.; Ribeiro da Silva, M. A. V. *Thermochim. Acta* **2004**, *415*, 15–20.
(35) Frisch, M. J.; et al. *Gaussian 03*, revision C.02; Gaussian, Inc.: Pittsburgh, PA, 2004.
(36) Grimme, S. J. *J. Chem. Phys.* **2003**, *118*, 9095–9102.
(37) Pfaendtner, J.; Yu, X.; Broadbelt, L. J. *Theor. Chem. Acc.* **2007**, *118*, 881–898.
(38) Yu, X.; Pfaendtner, J.; Broadbelt, L. J. *J. Phys. Chem. A* **2008**, *112*, 6772–6782.
(39) Yu, X.; Levine, S. E.; Broadbelt, L. J. *Macromolecules* **2008**, *41*, 8242–8251.
(40) Hua, G.; Li, Y.; Slawin, A. M. Z.; Woollins, J. D. *Dalton Trans.* **2007**, 1477–1480.
(41) Lutz, M.; Spek, A. L.; Bonnet, S.; Klein Gebbink, R. J. M.; Koten, G. CCDC 609800, Private Communication, 2006.
(42) Allen, F. H.; Kennard, O.; Watson, D. G.; Orpen, G.; Brammer, L.; Taylor, R. *J. Chem. Soc., Perkin Trans. 2* **1987**, S1.
(43) *CODATA Key Values for Thermodynamics*; Cox, J. D., Wagman, D. D., Medvedev, V. A., Eds.; Hemisphere: New York, 1989.
(44) Merrick, J. P.; Moran, D.; Radom, L. *J. Phys. Chem. A* **2007**, *111*, 11683–11700.
(45) Blanquart, G.; Pitsch, H. *J. Phys. Chem. A* **2007**, *111*, 6510–6520.
(46) Sinha, P.; Boesch, S. E.; Gu, C.; Wheeler, R. A.; Wilson, A. K. *J. Phys. Chem. A* **2004**, *108*, 9213–9217.
(47) Roux, M. V.; Temprado, M.; Chickos, J. S.; Nagano, Y. *J. Phys. Chem. Ref. Data* **2008**, *37*, 1855–1996.
(48) Kruif, C. G. *J. Chem. Thermodyn.* **1980**, *12*, 243–248.
(49) Chirico, R. D.; Knipmeyer, S. E.; Nguyen, A.; Steele, W. V. *J. Chem. Thermodyn.* **1989**, *21*, 1307–1331.
(50) Ribeiro da Silva, M. A. V.; Santos, L. M. N. B. F.; Lima, L. M. S. S. *J. Chem. Thermodyn.* **2008**, *40*, 375–385.
(51) Ribeiro da Silva, M. A. V.; Santos, L. M. N. B. F.; Lima, L. M. S. S. *J. Chem. Thermodyn.* **2010**, *42*, 134–139.
(52) Swendsen, R. H. *Entropy* **2008**, *10*, 15–18.
(53) Kramer, G. M.; Scouten, C. G.; Kastrup, R. V.; Ernst, E. R.; Pictroski, C. F. *J. Phys. Chem.* **1989**, *93*, 6257–6260.
(54) Estrada, E.; Avnir, D. *J. Am. Chem. Soc.* **2003**, *125*, 4368–4375.
(55) Brown, R. J. C.; Brown, R. F. C. *J. Chem. Educ.* **2000**, *77*, 724–731.
(56) Gilbert, A. S. *Thermochim. Acta* **2007**, *452*, 135–139.
(57) Abramowitz, R.; Yalkowsky, S. H. *Pharm. Res.* **1990**, *7*, 942–947.
(58) Lin, S.-K. *J. Chem. Inf. Comput. Sci.* **1996**, *36*, 367–376.
(59) Pinal, R. *Org. Biomol. Chem.* **2004**, *2*, 2692–2699.
(60) Watson, L. A.; Eisenstein, O. *J. Chem. Educ.* **2002**, *79*, 1269–1277.
(61) Wei, J. *Ind. Eng. Chem. Res.* **1999**, *38*, 5019–5027.
(62) Dannenfelser, R.-M.; Yalkowsky, S. H. *Ind. Eng. Chem. Res.* **1996**, *35*, 1483–1486.
(63) Breuer, J.; Avnir, D. *J. Chem. Phys.* **2005**, *122*, 074110−1 074110−10.
(64) Maczek, A. *Statistical Thermodynamics*; Oxford University Press: New York, 2008; p 19.
(65) Atkins, P.; de Paula, J. *Physical Chemistry*, 7th ed.; Oxford University Press: New York, 2002; p 650.
(66) Mayer, J. E.; Brunauer, S.; Mayer, M. G. *J. Am. Chem. Soc.* **1933**, *55*, 37–53.
(67) McQuarrie, D. A.; Simon, J. D. *Physical Chemistry: A Molecular Approach*; University Science Books: Sausalito, CA, 1997.
(68) Williams, D. E.; Xiao, Y. *Acta Crystallogr.* **1993**, *A49*, 1–10.
(69) Charbonneau, G.-P.; Delugeard, Y. *Acta Crystallogr.* **1977**, *B33*, 1586–1588.
(70) Aikawa, S.; Maruyama, Y. *Acta Crystallogr.* **1978**, *B34*, 2901–2904.
(71) Lima, C. F. R. A. C.; Gomes, L. R.; Santos, L. M. N. B. F.; Low, J. N. CCDC 782202.
(72) Rietveld, H. M.; Maslen, E. N.; Clews, C. J. B. *Acta Crystallogr.* **1970**, *B26*, 693–706.
(73) Lin, Y. C.; Williams, D. E. *Acta Crystallogr.* **1975**, *B31*, 318–320.
(74) Pascal, R. A., Jr. *Chem. Rev.* **2006**, *106*, 4809–4819.